Binary masses and luminosities with Gaia DR3

S. Chevalier, Carine Babusiaux, T. Merle, Frédéric Arenou

A&A 678, A19 (2023)
https://doi.org/10.1051/0004-6361/202347111

Astronomy & Astrophysics

Binary masses and luminosities with *Gaia* DR3⋆

S. Chevalier[1,2,3], C. Babusiaux[1], T. Merle[4,5], and F. Arenou[6]

[1] Univ. Grenoble Alpes, CNRS, IPAG, 38000 Grenoble, France
e-mail: carine.babusiaux@univ-grenoble-alpes.fr
[2] Kungliga Tekniska Hügskolan, 114 28 Stockholm, Sweden
[3] École Centrale de Lyon, 69130 Ecully, France
[4] Institut d'Astronomie et d'Astrophysique, Université Libre de Bruxelles (ULB), Brussels, Belgium
[5] Royal Observatory of Belgium, Avenue Circulaire 3, 1180 Brussels, Belgium
[6] GEPI, Observatoire de Paris, Université PSL, CNRS, 92190 Meudon, France

Received 6 June 2023 / Accepted 25 July 2023

ABSTRACT

Context. The recent third data release (DR3) of *Gaia* has brought some new exciting data about stellar binaries. It provides new opportunities to fully characterize more stellar systems and contributes to enriching our global knowledge of stellar behaviour.
Aims. By combining the new *Gaia* non-single stars catalogue with double-lined spectroscopic binaries (SB2), we can determine the individual masses and luminosities of the components. To fit an empirical mass-luminosity relation in the *Gaia G* band, lower-mass stars must be added. These masses can be derived using *Gaia*-resolved wide binaries combined with literature data.
Methods. Using the BINARYS tool, we combined the astrometric non-single star solutions in the *Gaia* DR3 with SB2 data from two other catalogues: the 9th Catalogue of Spectroscopic Binary orbits (SB9), and APOGEE. We also searched for low-mass stars that are resolved in *Gaia* with direct imaging and HIPPARCOS data or with a literature mass fraction.
Results. The combination of *Gaia* astrometric non-single star solutions with double-lined spectroscopic data enabled us to characterize 43 binary systems with SB9 and 13 systems with APOGEE. We furthermore derived the masses of 6 low-mass binaries that are resolved with *Gaia*. We then derived an empirical mass-luminosity relation in the *Gaia G* band down to 0.12 $\mathcal{M}_{\odot}$.

Key words. binaries: general – binaries: spectroscopic – binaries: visual – astrometry – stars: fundamental parameters

1. Introduction

The third data release (DR3) from the *Gaia* mission (Gaia Collaboration 2023b) provides non-single star solutions for hundreds of thousands sources for the first time (Gaia Collaboration 2023a). This is a new exciting dataset based on which new binary systems can be fully characterized, their dynamical masses and luminosities in particular.

Estimating stellar masses is a fundamental process with which the understanding of the stellar behaviour (luminosity, evolution, etc.) can be improved. This can mainly be achieved by characterizing binary systems, and this is the aim of this paper. The stars that can be fully characterized, such as those studied in this paper, are few, but they are crucial because they enable calibration of fundamental physical relations. These relations will then enable estimating the parameters of single stars or objects that are hard to reach, such as mass using a mass-luminosity relation for main-sequence stars. The mass-luminosity relation is derived from fully characterized star systems, the masses and luminosities of which are known for both components. Knowing the dynamical masses also enables constraining other characteristics of the stars, such as their age, through isochrone fitting.

One of the main purposes of this paper is to use these new *Gaia* DR3 data to provide new dynamical masses and a first mass-luminosity relation in the *G* band. Empirical mass-luminosity relations are mostly provided in the near-infrared range because it does not depend on the metallicity as much as the visible range (e.g. Delfosse et al. 2000; Benedict et al. 2016; Mann et al. 2019). In the visible range, empirical mass-luminosity relations are provided in the *V* band (e.g. Delfosse et al. 2000; Benedict et al. 2016).

Masses of double-lined spectroscopic binaries (SB2) have been obtained so far mainly through eclipsing binaries and a smaller sample of visually resolved binaries. Visually resolved binaries have the advantage of also providing a measure of the parallax of the system (e.g. Pourbaix 2000). Masses can also be estimated together with the luminosity of the stars through the astrometric motion of the photocentre. However, this motion was too small in general to be detected by HIPPARCOS (ESA 1997; see e.g. Jancart et al. 2005), except in a few cases (Arenou et al. 2000). An observing program of SB2 has been initiated in 2010 to allow the determination of masses at the 1% level using future *Gaia* astrometric orbits (Halbwachs et al. 2020). The new *Gaia* DR3 astrometric orbits allow the determination of new masses of SB2 systems, as was done between the *Gaia* SB2 and astrometric orbital solutions in Gaia Collaboration (2023a). However, the astrometric motion affected the epoch radial velocity measures of *Gaia* (Babusiaux et al. 2023), leading to a poor goodness of fit of the solutions. They are therefore not considered here. Here, we combine *Gaia* astrometric data with double-lined spectroscopic data from the Apache Point Observatory Galactic Evolution Experiment (APOGEE; Kounkel et al. 2021) and the 9th Catalogue of Spectroscopic Binary orbits (SB9; Pourbaix et al. 2004) to derive the dynamical mass of each component as well as the flux of the components in the *G* band.

⋆ Full Tables 1–3 are available at the CDS via anonymous ftp to cdsarc.u-strasbg.fr (130.79.128.5) or via http://cdsarc.u-strasbg.fr/viz-bin/qcat?J/A+A/678/A19

Section 2 presents the data we used: the double-lined spectroscopic data (Sect. 2.1) and the astrometric solutions from *Gaia* (Sect. 2.2). Then the method we used to determine the binary masses is explained in Sect. 3. The results we obtained are discussed in Sect. 4. Section 5 is dedicated to the mass-luminosity relation. We first present six low-mass stars resolved by *Gaia* with direct-imaging data (Sect. 5.1) and then the fit of the mass-luminosity relation (Sect. 5.2).

2. Data

2.1. Double-lined spectroscopic data

Spectroscopic data have been obtained by measuring the Doppler effect of the stellar system. The stellar motion induces a periodic translation of their spectrum depending on their motion in the line of sight from the Earth. For double-lined spectroscopy, the motion of the two sources of the binary are well identified, and the ratio of the amplitude of the radial velocity motion provides the mass ratio of the stellar system. Estimating the mass requires knowing the inclination, which cannot be obtained from the spectroscopic orbit. We used double-lined spectroscopic data originating from two catalogues: APOGEE and SB9.

The SB9 catalogue (Pourbaix et al. 2004) is a huge compilation of spectroscopic orbits from the literature over the past decades. It lists about 5000 orbits together with the input radial velocities used to derive the orbit. Fifty-five of these have available epoch radial velocities and a *Gaia* astrometric orbit counterpart. The compatibility of the orbital solutions provided by *Gaia* astrometry and SB9 spectroscopy was first checked to remove triple systems. We required a consistency at 10σ for the periods P,

$$|P_{Gaia} - P_{SB9}| < 10\sqrt{\sigma^2_{P_{Gaia}} + \sigma^2_{P_{SB9}}}. \quad (1)$$

We note that a consistency at 5σ would have removed the well-behaved solution *Gaia* DR3 1528045017687961856 (HIP 62935). The compatibility of the eccentricity within 10σ was also checked (as in Eq. (1)), but did not remove any stellar system. In this way, 43 SB9 binaries were selected.

The APOGEE survey (Majewski et al. 2017) is conducted with two high-resolution spectrographs, covering the spectral band between 1.51 and 1.7 µm. The data used in this paper originated from Kounkel et al. (2021), who detected 7273 double-lined spectroscopic systems. One hundred eighty-three star systems have been found to have both double-lined SB2 spectroscopy data in APOGEE and an astrometric orbital solution in the *Gaia* non-single star (NSS) catalogue, but only 126 with more than one APOGEE epoch have been kept.

Only one orbit of these star systems could be solved through spectroscopy alone by Kounkel et al. (2021): *Gaia* DR3 702393458327135360 (HD 80234). The direct combination of these spectroscopic parameters with *Gaia* astrometry was achieved by Gaia Collaboration (2023a) to derive the masses of this system. For the other stars with a *Gaia* NSS solution counterpart, the constraints from the astrometric orbit can be used to extract the mass ratio from the raw radial velocity curves.

The SB9 radial velocity curves have a much wider observation time range than APOGEE. There are enough data from various epochs for an independent fit of the orbit with spectroscopy alone. The orbital parameters are directly given with their associated errors in the catalogue. This is not the case for our APOGEE sample, except for *Gaia* DR3 702393458327135360 (HD 80234).

2.2. Gaia DR3 astrometric orbits

Astrometric data are obtained by observing the corkscrew-like motion of the photocentre, that is, the apparent light source of the binary system. This provides the required inclination, but also the parallax, and, combined with an SB2 solution, the flux ratio.

Here the astrometric data are given by the orbital solutions from the *Gaia* DR3 non-single star solutions catalogue. This new catalogue has a significantly increased number and precision for binary system solutions (Gaia Collaboration 2023a). The catalogue provides several types of solutions depending on the collected data and the detection method or instrument used, that is, eclipsing, spectroscopic and astrometric solutions, and potential combinations of these. In this paper, we only use the astrometric solutions. Twenty-one objects in our final sample have a combined AstroSpectroSB1 solution for which only the astrometric part is taken into account. In *Gaia* DR3, the orbit is not described by the Campbell elements (semi-major axis, inclination, node angle, and periastron angle), but by the Thiele-Innes coefficients (Halbwachs et al. 2023).

3. Data processing

While for SB9 the orbital parameters are known and the computation of the masses can be derived directly (Appendix A), we return to the raw spectroscopic data here to improve the correlations between the parameters.

We combined pectroscopy and astrometry with the code BINARYS (Leclerc et al. 2023). BINARYS can combine HIPPARCOS and/or *Gaia* absolute astrometric data with relative astrometry and/or radial velocity data. It has been updated to handle *Gaia* NSS solutions, and its core, which computes the likelihoods, is available online[1]. It needs initial values and uses the automatic differentiation code Template Model Builder (TMB; Kristensen et al. 2016) to find the maximum likelihood. The output is the estimated orbital parameters with the associated covariance matrix, together with a convergence flag. Because Monte Carlo techniques cannot be used with the astrometric Thiele-Innes coefficients of *Gaia* DR3 (see Sect. 6.1 of Babusiaux et al. 2023), the Markov chain Monte Carlo (MCMC) option of BINARYS cannot be used in this study, while the TMB automatic differentiation is consistent with the local linear approximation result.

BINARYS provides the primary semi-major axis a_1, the mass ratio $q = \mathcal{M}_2/\mathcal{M}_1$, and the period P with their associated covariance matrix for all the orbital parameters. This enables us to derive the primary and secondary masses (see Eqs. (2) and (3)) with the associated errors (Appendix B),

$$\mathcal{M}_1 = \frac{a_1^3\,(1+q)^2}{P^2\,q^3} \quad (2)$$

$$\mathcal{M}_2 = \frac{a_1^3\,(1+q)^2}{P^2\,q^2}, \quad (3)$$

where the period P is given in years, a_1 is given in au, and the masses $\mathcal{M}$ are given in solar masses $\mathcal{M}_\odot$. It also gives the flux fraction of the secondary β in the G spectral band,

$$\beta = \frac{F_2}{F_1 + F_2} = \frac{q}{1+q}\left(1 - \frac{a_0}{a_1}\right), \quad (4)$$

where a_0 is the semi-major axis of the photocentre in the same unit as a_1 (see Appendix A).

[1] https://gricad-gitlab.univ-grenoble-alpes.fr/ipag-public/gaia/binarys

3.1. SB9

The radial velocity epoch data for each component, the orbital astrometric solution from *Gaia* NSS, and initial parameters were used as input for BINARYS. They were chosen for SB9 to be the result of the direct calculation process (Appendix A).

Inflation of the raw radial velocity uncertainties is quite often needed, either due to an under-estimation of the formal errors, a template mismatch, or stellar variability effects. We therefore applied a procedure similar to Halbwachs et al. (2020) to correct for the uncertainties.

We first applied the variance weight factors w provided in the SB9 database. They were provided by some studies that combined different observations and give their relative weights. We therefore started from the weighted uncertainties $\sigma = \frac{\sigma_0}{\sqrt{w}}$.

Then these uncertainties were adjusted using the goodness-of-fit estimator F2 (Wilson & Hilferty 1931),

$$\mathrm{F2} = \left(\frac{9\nu}{2}\right)^{1/2}\left[\left(\frac{\chi^2}{\nu}\right)^{1/3} + \frac{2}{9\nu} - 1\right], \tag{5}$$

where ν is the number of degrees of freedom, and χ^2 is the weighted sum of the squares of the differences between the predicted and observed values. The radial velocity uncertainties were scaled to obtain F2 = 0 *i.e.* $\chi^2 = \chi^2_0$,

$$\chi^2_0 = \nu\left(1 - \frac{2}{9\nu}\right)^3. \tag{6}$$

The corrected uncertainties are then

$$\sigma_{\mathrm{corr}} = \sqrt{\frac{\chi^2}{\chi^2_0}} \times \sigma. \tag{7}$$

This correction factor was applied three times: the uncertainties were adjusted once independently for each component with an SB1 correction, and they were then adjusted again together with a SB2 correction over the whole system.

The process requires the number of the degrees of freedom to be positive, that is, to have more epochs than parameters to fit. This was always the case, except for *Gaia* DR3 1480959875337657088 (HIP 69885), which has only two epochs for the primary and the secondary. No uncertainty correction was applied here. In the literature, an orbit fit could have been achieved using additional blended radial velocity epochs, which could not be used here. For this star, the orbital parameters are mainly driven by the *Gaia* NSS solution. Four other star systems do not have enough radial velocity epochs for the secondary to have the SB1 solution that is necessary to apply the correction process: *Gaia* DR3 1441993625629660800, 1517927895803742080, 4145362250759997952, and 4354357901908595456 (HIP 66511, HIP 61436, HD 163336 B, and HIP 81170, respectively). For these, the two other error correction factors, SB1 primary and SB2, were still applied, and the χ^2 of the final solution on the secondary was checked to be small.

About ten star systems have had a significant SB1 correction factor over the primary and/or the secondary, with $\sqrt{\frac{\chi^2}{\chi^2_0}} > 1.3$.

3.2. APOGEE

Similarly, BINARYS was provided the APOGEE radial velocity epoch data for each component, and the orbital astrometric solution from *Gaia* NSS. Because the spectroscopic orbit is not known for APOGEE, the BINARYS code had to be initialized with various initial parameters. We used sampled initial values of $\mathcal{M}_1$ from 0.6 to 1.4 solar mass with a 0.2 step, $\mathcal{M}_2$ from 0.6 to 1.4 solar mass with a 0.2 step (keeping $\mathcal{M}_2 \leq \mathcal{M}_1$), and β from 0 to 0.5 with a 0.1 step. Because the direction of motion is set by the spectroscopy, we also tried different configurations for the node angle, adding or not a π angle to both the node angle Ω and the argument of periastron ω to the *Gaia* astrometric orbit values. For each system, $15 \times 6 \times 2 = 180$ initial configurations were tested for each star system.

The convergence of TMB towards a good solution is not expected for every system: many will be triple systems for which the short-period binary is seen by APOGEE and the longer-period binary is seen by *Gaia*. Each TMB output corresponding to an initial configuration of a given star system must then fit the following criteria to be kept: it must converge, with a goodness-of-fit estimator F2 < 5, and the flux fraction of the secondary should be within the interval $[0;\ 0.5]$ at 3σ. The star system was kept only when these conditions were met by at least 10% of the 180 initial configurations tested. Then, for each star system, only the solution obtained for more than 80% of the cases for which TMB converged was kept. When no such solution existed, the star system was rejected.

Thirty-five of the 126 star systems we studied remained at this point. Due to the small number of radial velocity epochs, the precision of the solution may be too low on the masses to be interesting even though the convergence is good. For the final selection, we kept only stars with $\frac{\sigma_q}{q} < 0.5$, $\frac{\sigma_{\mathcal{M}_1}}{\mathcal{M}_1} < 0.5$, and $\sigma_{\mathcal{M}_1} < 1\,\mathcal{M}_\odot$. This led to 13 systems. This selection step was only applied for APOGEE because the selection over SB9 star systems was performed through the compatibility of periods.

4. Results

We obtained the dynamical masses and flux fraction of the individual stars of 56 binary systems by combining *Gaia* DR3 NSS astrometric solutions with SB2 solutions from SB9 (43 systems) and APOGEE (13 systems). Figure 1 provides the position of the binaries we characterized in the HR diagram.

The results obtained through the orbit fitting process are given in Table 1 for SB9.

The uncertainties on the masses of the binary system *Gaia* DR3 3954536956780305792 (HIP 61816) are extremely large, with $\frac{\sigma_{\mathcal{M}_1}}{\mathcal{M}_1} \approx 1$. These results therefore cannot be used. We expect this result to be a consequence of the lack of constraints over the inclination for this system, which is $i = 27.5 \pm 12.7°$. Being compatible with 0 at less than 3σ, the masses are much less constrained as well, leading to the large uncertainties.

The characterization of the binaries from APOGEE is detailed in Table 2. A particular case to be considered is *Gaia* DR3 839401128363085568 (LP 129-155). The results lead to $\mathcal{M}_1 = 1.49 \pm 0.44\,\mathcal{M}_\odot$, $\mathcal{M}_2 = 1.34 \pm 0.37\,\mathcal{M}_\odot$, and $\beta = 0.40 \pm 0.03$, with F2 $= 2.5$. These parameters make the system an outlier in the mass-luminosity relation. Although MCMC is not adapted to the Thiele-Innes handling, we tested a short MCMC on this star that indicated the presence of another solution with lower mass values. This binary system is the only one in our sample with a low eccentricity consistent with zero at 1σ. The system was additionally tested with an eccentricity fixed to 0, corresponding to a circular orbit. The result we obtained fits the mass-luminosity relation much

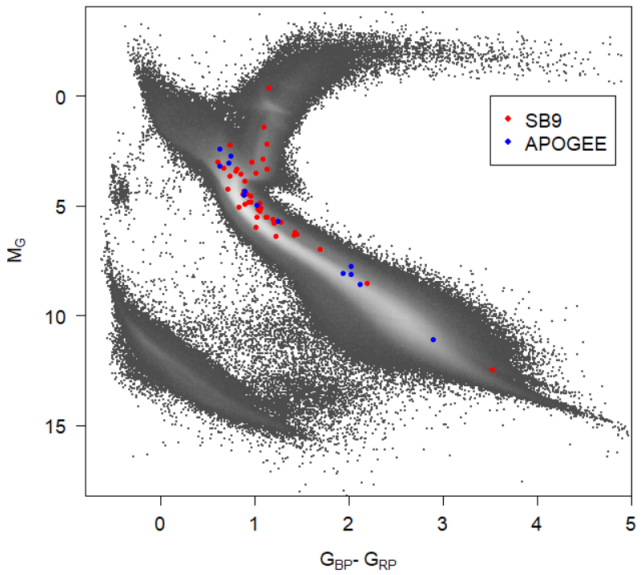

Fig. 1. Hertzsprung-Russel diagram of the characterized binaries. The absolute magnitude of the unresolved binary in the G band M_G is plotted as a function of the colour $G_{BP} - G_{RP}$. The blue dots correspond to the APOGEE binaries, and the red dots correspond to the SB9 binaries. They are overplotted on the low-extinction *Gaia* DR3 HR diagram (in grey).

better, despite its slightly larger F2, and this solution is kept in Table 2.

Because *Gaia* provides the G magnitude of the binary system, the individual absolute magnitude in the G band can be deduced for each star using A_G, the extinction in the G band derived from the 3D extinction map of Lallement et al. (2022), and using the *Gaia* DR3 extinction law[2],

$$M_{G_1} = G + 2.5\log_{10}\left(\frac{1}{1-\beta}\right) + 5 + 5\log_{10}\left(\frac{\varpi}{1000}\right) - A_G \quad (8)$$

$$M_{G_2} = G + 2.5\log_{10}\left(\frac{1}{\beta}\right) + 5 + 5\log_{10}\left(\frac{\varpi}{1000}\right) - A_G, \quad (9)$$

where ϖ is the parallax in mas.

To estimate the uncertainties of these absolute magnitudes (see Appendix B), a 10% relative error on the extinction with a minimum error of 0.01 mag was assumed, and a 0.01 mag error was added in quadrature to the G formal magnitude errors. The extinction term A_G remained negligible for 90% of our sample, with a maximum A_G of 0.03 for APOGEE and 0.15 for SB9.

Figure 2 for SB9 and Fig. 3 for APOGEE show the positions of all the individual stars we characterized in the mass-luminosity diagram. They are overplotted on the PARSEC solar-metallicity isochrones (Bressan et al. 2012).

Almost all the stars are compatible with the isochrones at 3σ. For SB9, one star can be considered as an outlier, *Gaia* DR3 3427930123268526720 (GJ 220), which is the only system of the SB9 sample with F2 > 5. For APOGEE, one main outlier exists, *Gaia* DR3 5285071954833306368 (HD 50199). This is still compatible with the isochrones at less than 5σ. Nothing specific has been found about this system to justify its surprising position in the diagram.

[2] https://www.cosmos.esa.int/web/Gaia/edr3-extinction-law

The goodness of fit of the *Gaia* DR3 astrometric solution is higher than 10 for 11 systems, but none are outliers in the mass-luminosity relation, in the F2 of the combined fit, or in the relation between the flux fraction and the mass ratio. We therefore decided to keep these systems in our sample for the mass-luminosity relation study in Sect. 5.

4.1. Comparison with the direct calculation method for SB9

As a sanity check, we compared the masses obtained with the orbit-fitting process (Table 1) to those obtained through direct calculation, that is, using the orbital parameters provided by SB9 directly to derive the mass functions without returning to the raw data, as detailed in Table A.1.

Returning to the raw spectroscopic data allowed us to take the correlations between the spectroscopic parameters into account and then gain a better estimation of the orbital parameters and their uncertainties. Moreover, a correction process was applied to the uncertainties of the radial velocity epochs, which made them more realistic.

Figure 4 presents the distribution of the compatibility (in σ) between the masses obtained for the orbit-fitting process and the direct calculation. The compatibility is defined as

$$\text{compatibility} = \frac{\mathcal{M}_{OF} - \mathcal{M}_{DC}}{\max(\sigma_{OF}, \sigma_{DC})}, \quad (10)$$

where $\mathcal{M}_{OF}$ is the mass obtained through orbit fitting, and $\mathcal{M}_{DC}$ is the mass obtained through direct calculation.

As expected, this shows that the results are nicely compatible, but with a difference that is not fully negligible in some cases.

Figure 5 provides the uncertainties over the masses obtained with one method with respect to the other. The majority of the mass uncertainties lie below the identity line, meaning that the uncertainties coming from the direct calculation process are generally higher than those from orbit fitting. This confirms that the uncertainties over the orbital parameters are often reduced when accounting for the correlations between them.

A few points have slightly larger uncertainties through the orbit-fitting process. This is the result of the correction process we applied to the uncertainties (see Eq. (7)).

One noteworthy case is *Gaia* DR3 4145362250759997952 (HD 163336 B), for which the difference between the uncertainties is quite large. The radial velocity data contain only three epochs for the secondary. Thus, we can expect a strong correlation between the SB9 orbital parameters. We performed an MCMC over the raw spectroscopic data alone and confirm that strong correlations appear and that the distribution is strongly asymmetric. This explains the strong improvement we obtained by including the knowledge of the *Gaia* orbit in the spectroscopic fit.

4.2. Reference comparison

Three star systems from our SB9 sample are identified as SB2 in the *Gaia* DR3 catalogue with direct masses derived by Gaia Collaboration (2023a). While our mass estimates are consistent with those of *Gaia* DR3 1067685718250692352 (HIP 45794) and *Gaia* DR3 2035577729682322176 (HIP 97640), *Gaia* DR3 595390807776621824 HIP 42418) is a 5σ outlier. It has a photocentre semi-major axis a_0 of 3.4 mas, while the other two stars have a smaller $a_0 \sim 0.8$ mas, suggesting that the astrometric motion impacted the spectroscopic measure, as suggested by Babusiaux et al. (2023). The reason

Table 1. Solutions from the combination of *Gaia* NSS astrometric solutions with SB9 double-lined spectroscopy.

Gaia DR3 ID	q	σ_q	$\mathcal{M}_1$	$\sigma_{\mathcal{M}_1}$	$\mathcal{M}_2$	$\sigma_{\mathcal{M}_2}$	β	σ_β	F2	Ref.
48197783694869760	0.6771	0.0124	0.9707	0.0423	0.6573	0.0190	0.0936	0.0030	1.32	1
69883417170175488	0.9793	0.0224	0.8271	0.0289	0.8100	0.0273	0.3976	0.0084	−0.03	2
308256610357824640	0.6970	0.0099	0.4283	0.2000	0.2985	0.1393	0.2770	0.0232	−0.15	3
478996438146017280	0.9212	0.0064	0.8112	0.0249	0.7473	0.0228	0.3879	0.0030	1.25	4
544027809281308544	0.8336	0.0178	0.9465	0.0510	0.7890	0.0317	0.1363	0.0072	0.01	5
595390807776621824	0.8822	0.0061	0.7877	0.0105	0.6948	0.0066	0.3123	0.0017	−0.03	6
660622010858088320	0.8707	0.0367	0.7304	0.0607	0.6360	0.0341	0.2252	0.0081	1.01	5
827608625636174720	0.9403	0.0129	0.7357	0.0392	0.6917	0.0367	0.4076	0.0045	0.29	7
882872210352301568	0.5027	0.0026	1.0044	0.0123	0.5049	0.0036	0.0257	0.0038	−0.07	8
1067685718250692352	0.8884	0.0036	1.0279	0.0125	0.9132	0.0101	0.3035	0.0048	0.10	9
1074883087005896320	0.9388	0.0261	0.6640	0.0393	0.6233	0.0326	0.3977	0.0068	1.11	10
1324699172583973248	0.8839	0.0087	1.3136	0.0476	1.1611	0.0376	0.3167	0.0039	0.40	11
1441993625629660800	0.8344	0.0128	1.1033	0.0455	0.9205	0.0293	0.0706	0.0132	−0.10	12
1480959875337657088	0.9351	0.0771	0.8679	0.1330	0.8116	0.0925	0.2884	0.0180	0.77	13
1517219363639758976	0.8198	0.0062	1.0650	0.0405	0.8731	0.0313	0.1576	0.0075	1.55	14
1517927895803742080	0.9076	0.0148	0.6354	0.0251	0.5767	0.0183	0.3546	0.0037	1.75	7
1528045017687961856	0.6793	0.0029	1.1179	0.0285	0.7593	0.0185	0.0623	0.0045	2.30	15
1615450866336763904	0.7864	0.0106	1.0138	0.0396	0.7973	0.0261	0.1317	0.0044	0.14	16
1918953867019478144	0.9308	0.0007	1.0465	0.0050	0.9741	0.0047	0.3866	0.0014	0.63	17
2012218158438964224	0.9486	0.0150	2.3368	0.1644	2.2168	0.1509	0.3589	0.0064	0.92	18
2035577729682322176	0.9024	0.0089	0.7027	0.0417	0.6341	0.0374	0.3227	0.0056	−0.16	19
2067948245320365184	0.7863	0.0006	0.8374	0.0023	0.6584	0.0017	0.1521	0.0014	0.48	17
2129771310248902016	0.9071	0.0183	0.7408	0.0399	0.6720	0.0302	0.3184	0.0048	−0.16	10
2185171578009765632	0.9629	0.0082	1.2178	0.0299	1.1727	0.0333	0.4436	0.0033	1.28	17
2198442167969655296	0.7508	0.0152	0.9844	0.0416	0.7391	0.0189	0.1963	0.0033	0.65	10
3283823387685219328	0.7419	0.0004	0.9864	0.0112	0.7319	0.0083	0.1478	0.0031	0.37	20
3312631623125272448	0.7062	0.0024	0.9920	0.0304	0.7005	0.0215	0.1249	0.0051	1.54	21
3366718833479009408	0.6407	0.0022	1.0494	0.0102	0.6724	0.0051	0.0155	0.0028	0.18	8
3409686270424363008	0.7076	0.0031	0.7927	0.0139	0.5610	0.0087	0.1086	0.0028	2.07	17
3427930123268526720 [(a)]	0.3311	0.0047	0.8066	0.0760	0.2671	0.0248	0.0616	0.0066	5.23	3
3536759371865789568	0.8392	0.0212	1.6490	0.0899	1.3838	0.0492	0.2000	0.0061	0.62	22
3549833939509628672	0.9406	0.0195	0.9450	0.0384	0.8889	0.0249	0.3567	0.0051	0.19	22
3931519127529822208	0.7750	0.0260	1.0791	0.0762	0.8363	0.0342	0.1403	0.0045	1.19	23
3935131126305835648	0.7039	0.0022	1.4860	0.0744	1.0460	0.0523	0.1374	0.0052	0.08	20
3954536956780305792	0.9053	0.0094	0.7713	0.7626	0.6982	0.6904	0.3262	0.0600	0.49	5
3964895043508685312	0.8650	0.0084	0.7531	0.1654	0.6514	0.1426	0.2201	0.0196	−0.09	17
4145362250759997952	0.6960	0.0216	0.9414	0.0611	0.6552	0.0261	0.0757	0.0046	0.16	24
4228891667990334976	0.8629	0.0057	1.0907	0.0588	0.9412	0.0502	0.2872	0.0038	4.10	25
4354357901908595456	0.5832	0.0194	0.7005	0.0509	0.4085	0.0177	0.0606	0.0041	0.18	26,27
4589258562501677312	0.8201	0.0317	0.6679	0.0628	0.5478	0.0395	0.2924	0.0085	−0.13	5
5762455439477309440	0.8041	0.0327	0.8058	0.0674	0.6480	0.0333	0.1768	0.0076	0.20	5
6244076338858859776	0.8820	0.0076	0.7730	0.0135	0.6818	0.0101	0.2943	0.0023	0.86	10
6799537965261994752	0.9000	0.0017	0.9036	0.0092	0.8132	0.0083	0.3267	0.0024	1.32	24

Notes. q is the mass ratio, $\mathcal{M}_1$ is the mass of the primary, $\mathcal{M}_2$ is the mass of the secondary (in $\mathcal{M}_\odot$) and β is the flux fraction of the secondary. σ_q, $\sigma_{\mathcal{M}_1}$, $\sigma_{\mathcal{M}_2}$ and σ_β are their associated uncertainties. F2 is the goodness-of-fit estimator. Ref gives the reference of the raw radial velocity data used in the fit, as provided by SB9. [(a)]High F2, removed from the Sect. 5 study. Full table including the correlations and the orbital parameters is available at the CDS.

References. (1) Tomkin (2005); (2) Mermilliod et al. (2009); (3) Baroch et al. (2018); (4) Fekel et al. (1994); (5) Goldberg et al. (2002); (6) Griffin (2009); (7) Sperauskas et al. (2019); (8) Fekel et al. (2015); (9) Ginestet & Carquillat (1995); (10) Halbwachs et al. (2018); (11) Griffin (2011); (12) Griffin (1990); (13) Halbwachs et al. (2012); (14) Griffin (2008); (15) Kiefer et al. (2016); (16) Griffin (2013); (17) Kiefer et al. (2018); (18) Griffin (1993); (19) Imbert (2006); (20) Halbwachs et al. (2020); (21) Tomkin (2007); (22) Griffin (2006); (23) Griffin (2012); (24) Tokovinin (2019); (25) Griffin (2014); (26) Mazeh et al. (1997); (27) Mayor & Turon (1982).

is that the expected position of the spectra on the *Gaia* Radial Velocity Spectrometer (RVS) detectors is predicted by the standard five-parameter astrometric motion instead of the epoch astrometric motion, which would not be precise enough.

Masses were obtained combining a visual orbit with an SB2 orbit for *Gaia* DR3 2129771310248902016 (HIP 95575) by Piccotti et al. (2020) ($\mathcal{M}_1 = 0.670 \pm 0.069$, $\mathcal{M}_2 = 0.602 \pm 0.061$, compatible with our results within 1σ), for *Gaia* DR3 2067948245320365184 (HIP 101382) by Kiefer et al. (2018) ($\mathcal{M}_1 = 0.8420 \pm 0.0014$, $\mathcal{M}_2 = 0.66201 \pm 0.00076$, compatible with our results within 2σ), and for *Gaia* DR3 3283823387685219328 (HIP 20601) by Halbwachs et al. (2020)

Table 2. Solutions from the combination of *Gaia* NSS astrometric solutions with APOGEE double-lined spectroscopy.

Gaia DR3 ID	q	σ_q	$\mathcal{M}_1$	$\sigma_{\mathcal{M}_1}$	$\mathcal{M}_2$	$\sigma_{\mathcal{M}_2}$	β	σ_β	F2
839401128363085568 [(a)]	0.9143	0.0993	0.6225	0.1162	0.5692	0.0918	0.3865	0.0266	4.03
683525873153063680	0.9376	0.0496	0.5124	0.1037	0.4804	0.0951	0.3985	0.0167	1.72
702393458327135360	0.9398	0.0252	1.4875	0.5001	1.3980	0.4663	0.3871	0.0186	4.53
790545256897189760	0.8549	0.0846	0.4236	0.0870	0.3621	0.0618	0.2850	0.0263	1.20
794359875050204544	0.8824	0.1294	1.1746	0.3294	1.0365	0.2566	0.2676	0.0360	0.99
824315485231630592	0.9035	0.3744	0.9467	0.2152	0.8554	0.2087	0.3104	0.1036	3.92
901170214141646592	0.8396	0.1134	0.9309	0.2506	0.7815	0.1951	0.2330	0.0404	0.46
1267970076306377344	0.6633	0.0586	1.1378	0.2014	0.7547	0.0912	0.0703	0.0157	0.61
1636132061580415488	0.7176	0.1342	1.1046	0.4127	0.7927	0.2574	0.1488	0.0446	3.24
2134829544776833280	0.7721	0.0680	0.8751	0.1245	0.6757	0.0738	0.1505	0.0251	0.73
2705239237909520128	0.5293	0.1035	0.2336	0.0683	0.1236	0.0326	0.1993	0.0427	0.53
3847995791877023104	0.8387	0.0788	1.1446	0.2029	0.9600	0.1550	0.3167	0.0244	1.05
5285071954833306368 [(b)]	0.7905	0.1019	0.4609	0.1058	0.3643	0.0853	0.1499	0.0416	1.58

Notes. q is the mass ratio, $\mathcal{M}_1$ is the mass of the primary, $\mathcal{M}_2$ is the mass of the secondary (in $\mathcal{M}_\odot$), and β is the flux fraction of the secondary. σ_q, $\sigma_{\mathcal{M}_1}$, $\sigma_{\mathcal{M}_2}$, and σ_β are their associated uncertainties. F2 is the goodness-of-fit estimator. [(a)]Particular case for which the eccentricity was fixed to 0. [(b)]Mass-luminosity outlier, removed from the study in Sect. 5. The full table including the correlations and the orbital parameters is available at the CDS.

($\mathcal{M}_1 = 0.9798 \pm 0.0019\,\mathcal{M}_\odot$, $\mathcal{M}_2 = 0.72697 \pm 0.00094\,\mathcal{M}_\odot$, compatible with our results within 1σ). Halbwachs et al. (2020) combined the raw relative astrometry and spectroscopic data. They obtained a parallax at 4.4σ from the *Gaia* NSS parallax. We tested a combined fit with the radial velocity, interferometry from Halbwachs et al. (2020), and *Gaia* NSS solution and obtained a goodness of fit of F2 = 1.5, a parallax of $\varpi = 16.573 \pm 0.017$, and masses $\mathcal{M}_1 = 0.9816 \pm 0.0014\,\mathcal{M}_\odot$ and $\mathcal{M}_2 = 0.72808 \pm 0.00076\,\mathcal{M}_\odot$. This new parallax is at 3.4σ from that of Halbwachs et al. (2020) and reduces to 2.6σ when the *Gaia* DR3 parallax zero-point is taken into account (Lindegren et al. 2021). This highlights that SB2 stars with direct imaging will be excellent test cases for a validation of *Gaia* DR4 epoch data. The orbit fit for this binary is given in Fig. 6.

For APOGEE, the only star system for which masses have been obtained in the literature is the binary *Gaia* DR3 702393458327135360, which has been discussed in Sect. 2.1. This star was solved through spectroscopy alone (Kounkel et al. 2021) and was then combined with *Gaia* astrometry through a direct calculation process by Gaia Collaboration (2023a) to obtain $\mathcal{M}_1 = 1.14 \pm 0.38\,\mathcal{M}_\odot$, $\mathcal{M}_2 = 1.06 \pm 0.35\,\mathcal{M}_\odot$, and $F_2/F_1 = 0.567 \pm 0.071$. This is fully compatible with our results. The uncertainties reported here are larger than those of Gaia Collaboration (2023a). This may be due to a slight discrepancy between the orbital parameters of APOGEE and *Gaia*, specifically on the eccentricities, which are at 4σ from each other. This discrepancy leads to a high F2 of 4.6 in our solution and to higher uncertainties than what is obtained by a direct calculation. The orbit fit for the binary *Gaia* DR3 702393458327135360 (HD 80234) is given in Fig. 7. The difference in the observation time clearly appears in Figs. 6 and 7, where the lack of radial velocity epochs for APOGEE is rather obvious.

5. Mass-luminosity relation

The mass calculations presented above might enable an empirical fit of the mass-luminosity relation in the G band using the *Gaia* photometry. However, the masses we calculated do not provide satisfying constraints in the interesting region of the relation for low-mass stars ($\mathcal{M} < 0.7\,\mathcal{M}_\odot$). To fill in this part of the H-R diagram, we searched for low-mass stars that were resolved by *Gaia* and with direct-imaging data from the literature, following the work of Leclerc et al. (2023) on HIP 88745.

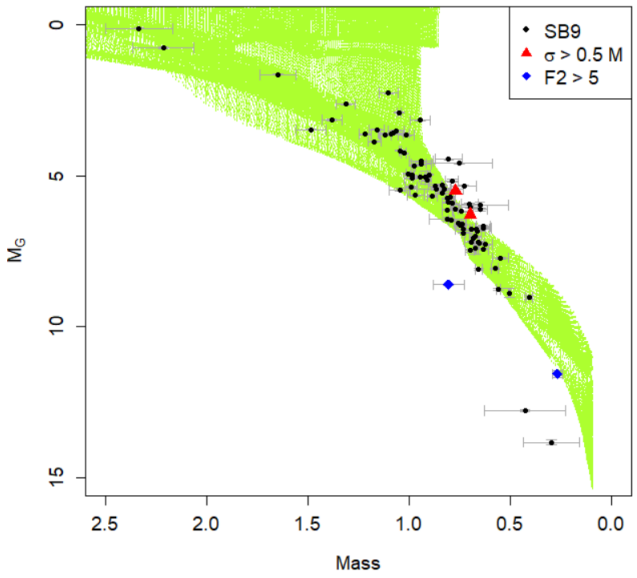

Fig. 2. Mass-luminosity diagram of the characterized stars from the combination of *Gaia* with SB9. The error bars at 1σ are given in grey. The absolute magnitude of the individual stars in the G band M_G is plotted as a function of the stellar mass (in $\mathcal{M}_\odot$). The black dots represent the stars, and the associated error bars at 1σ are shown in grey. The red triangles represent *Gaia* DR3 3954536956780305792, for which the uncertainties are really large and not represented here. The blue diamonds represent *Gaia* DR3 3427930123268526720, for which F2 > 5. They are overplotted on the solar-metallicity PARSEC isochrones (in green).

5.1. Low-mass systems resolved by Gaia with direct-imaging data

We found three spatially resolved stellar systems that were studied with direct imaging in Mann et al. (2019) that also

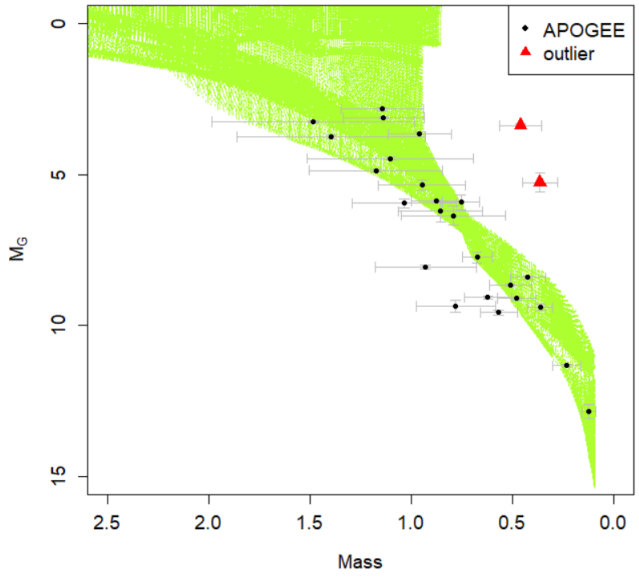

Fig. 3. Mass-luminosity diagram of the characterized stars from the combination of *Gaia* with APOGEE. The error bars at 1σ are given in grey. The absolute magnitude of the individual stars in the G band M_G is plotted as a function of the stellar mass (in $\mathcal{M}_\odot$). The black dots represent the stars, and the associated error bars at 1σ are shown in grey. The red triangles represent the outlier *Gaia* DR3 ID 5285071954833306368. They are overplotted on the isochrones (in green).

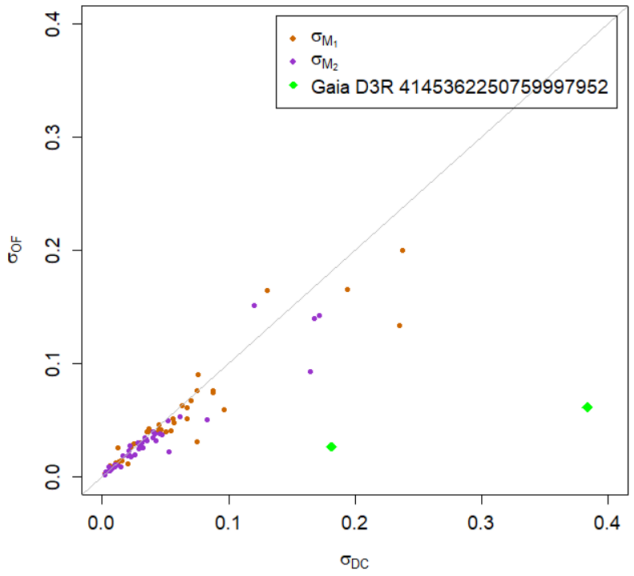

Fig. 5. Comparison of the uncertainties on the masses obtained by direct calculation (σ_{DC}) or by orbit fitting (σ_{OF}) for binaries from SB9. The primaries are given in orange, and secondaries are plotted in purple. The outlier star system *Gaia* DR3 4145362250759997952 is represented in green for its primary and secondary. The grey line is the identity line $y = x$.

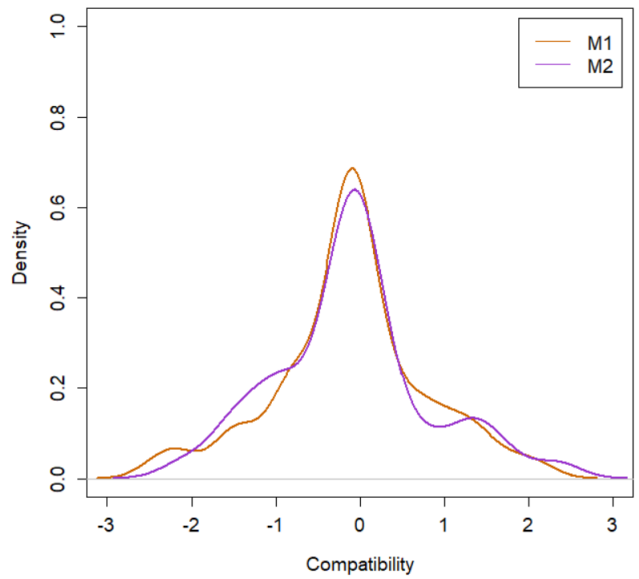

Fig. 4. Compatibility density of the masses obtained by direct calculation and by orbit fitting for SB9 binaries. The compatibility is given in σ. It is given in orange for primary masses and in purple for secondary masses.

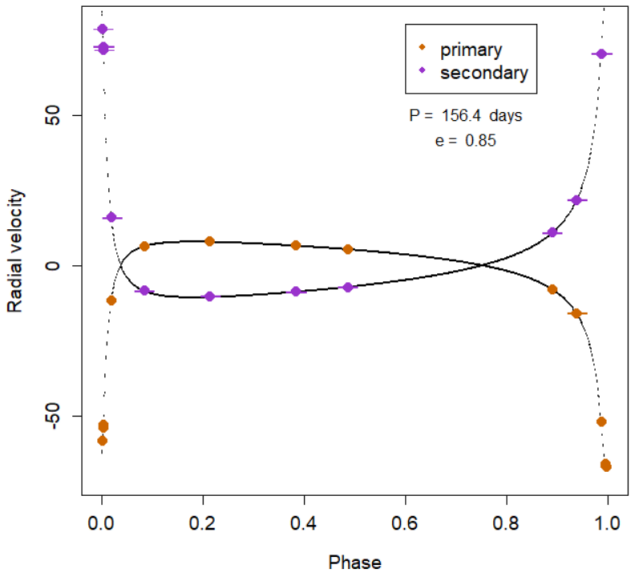

Fig. 6. Radial velocity fit for the binary system *Gaia* DR3 3283823387685219328 (HIP 20601) from SB9. The radial velocity (km s^{-1}) is plotted as a function of the phase. The orange dots correspond to the radial velocity epochs of the primary, and the purple dots show the radial velocity epochs for the secondary. The black curves represent the corresponding fits obtained by combining the SB9 epoch radial velocity with the *Gaia* DR3 NSS astrometric orbital solution with BINARYS.

have HIPPARCOS (van Leeuwen 2007) transit data (TD) and *Gaia*-resolved observations consistent with the direct-imaging data: Gl 330, Gl 860, and Gl 277. Gl 568 is not in the sample of Mann et al. (2019), but has direct-imaging data from McAlister et al. (1989) and Mason et al. (2018), and it was added to our sample. These four stars were analysed with BINARYS by combining the direct-imaging data with HIPPARCOS TD and *Gaia* astrometric parameters of both components following the method detailed in Leclerc et al. (2023). All *Gaia* solutions have a five-parameter solution except for Gl 330, for which the secondary component has a two-parameter solution, and Gl 860, for which both components only have a two-parameter solution. One HIPPARCOS TD outlier at 5σ had to be removed for both Gl 568 and Gl 227.

Two stars from the sample of Mann et al. (2019), Gl 65 and Gl 473, are resolved by *Gaia* with separations consistent with the visual orbit, but no HIPPARCOS data exist for them. However,

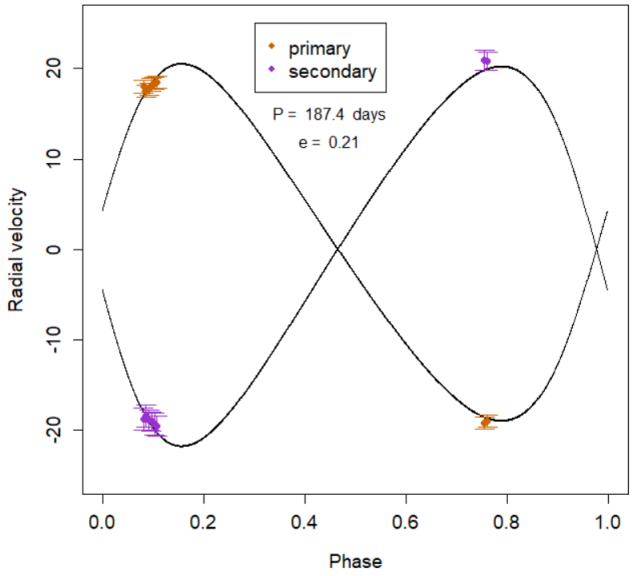

Fig. 7. Radial velocity fit for the binary system *Gaia* DR3 702393458327135360 (HD 80234) from APOGEE. The radial velocity ($\mathrm{km\,s^{-1}}$) is plotted as a function of the phase. The orange dots correspond to the radial velocity epochs of the primary, and the purple dots show the radial velocity epochs for the secondary. The black curves represent the corresponding fits obtained by combining the APOGEE epoch radial velocity with the *Gaia* DR3 NSS astrometric orbital solution with BINARYS.

these two stars have a literature mass fraction $B = \frac{\mathcal{M}_2}{\mathcal{M}_1+\mathcal{M}_2}$: for Gl 65, $B = 0.494 \pm 0.04$ from Geyer et al. (1988), and for Gl 473, $B = 0.477 \pm 0.008$ from Torres et al. (1999). We incorporated this information within BINARYS for these stars.

As our sample contains very nearby stars, we added the perspective acceleration terms in BINARYS following the description detailed in ESA (1997) and Halbwachs et al. (2023). We first computed the radial proper motion, that is, the relative change in distance per year, $\mu_r = V_r\varpi/A_Z$ in $\mathrm{yr^{-1}}$ with $A_Z = 9.7779222 \times 10^8$ mas yr km $\mathrm{s^{-1}}$. The perspective acceleration changes the along-scan abscissa ν (in mas) by adding

$$\Delta\nu = -\mu_r \Delta T \left(\frac{\partial \nu}{\partial \varpi}\varpi + \frac{\partial \nu}{\partial \mu_{\alpha^*}}\mu_{\alpha^*} + \frac{\partial \nu}{\partial \mu_\delta}\mu_\delta \right), \tag{11}$$

where ΔT is the epoch in years relative to the reference epoch for the astrometric parameters (i.e. 1991.25 for Hipparcos and 2016.0 for *Gaia* DR3). This $\Delta\nu$ was subtracted from the Hipparcos abscissa residuals and was added to the *Gaia*-simulated abscissa. However, the perspective acceleration was taken into account for DR3 for stars with a *Gaia* DR2 radial velocity or in the table of nearby Hipparcos stars with the radial velocity used for DR2[3]. Here, only the radial velocity for the A component of Gl 860 was applied for the DR3 processing, using the same $V_r = -33.94\,\mathrm{km\,s^{-1}}$ as we used. For Gl 65, we used $V_r = 39.04\,\mathrm{km\,s^{-1}}$ (Kervella et al. 2016), while for Gl 473, all literature V_r are consistent with zero. We checked that taking into account the perspective acceleration for our stars changed χ^2 only marginally.

The results obtained for these six stars are listed in Table 3. Our mass estimates are consistent with those from Kervella et al. (2016), Delfosse et al. (2000), and Benedict et al. (2016) for Gl 65, but we all used the same literature mass fraction. For Gl 473, using again the same literature mass fraction, our masses are consistent with Delfosse et al. (2000), but differ at 2.5σ from the values of Benedict et al. (2016). This is caused by the difference with the RECONS parallax they used. Our mass estimate for Gl 860 is consistent with that of Delfosse et al. (2000). To our knowledge, we derived the dynamical masses of the components of Gl 277, Gl 330, and Gl 568 for the first time.

5.2. Fitting the mass-luminosity relation

To fit the mass-luminosity relation, we implemented a TMB function that allowed us to take into account the uncertainties on both the mass and the magnitude, and more importantly, the correlations between the parameters of the two components of the same system (the calculation of the covariance is detailed in Appendix B). The true magnitudes of the stars were used as a random parameters: they were marginalized, that is, integrated out of the likelihood. The initial value of TMB was provided by a classical polynomial fit (`R lm` function). We selected only components with $M_G > 5$ to be used as input for the fit because the dependence on age for fainter magnitudes is well known to be too strong.

We tested several degrees for the polynomial and fitting the logarithm of the mass instead of the mass itself and used the Bayesian information criterion (BIC) to compare the models. The BIC favoured a polynomial of degree 4 to fit the log of the mass. The coefficients are listed in Table 4. The fit uncertainties were estimated through a bootstrap method, leading to uncertainties smaller than $0.015\,\mathcal{M}_\odot$ for magnitudes higher than $M_G > 6$, corresponding to masses $\mathcal{M} < 0.77\,\mathcal{M}_\odot$.

The fit is displayed in Fig. 8 together with the PARSEC, the Baraffe et al. (2015)[4], and the BASTI isochrones (Hidalgo et al. 2018)[5]. The age dependence of the mass-luminosity relation starts to be significant for all isochrones at $\gtrsim 0.6\,\mathcal{M}_\odot$, and our fit follows the oldest isochrones. For masses $<0.5\,\mathcal{M}_\odot$, our empirical relation indicates lower masses for a given luminosity than the PARSEC isochrones. Our results are consistent with the isochrones of Baraffe et al. (2015), except in the low-mass region, where we find slightly higher masses for a given luminosity.

6. Conclusion

We have estimated the masses of binary systems by combining the astrometric orbits from *Gaia* DR3 with spectroscopy, 43 star systems from SB9, and 13 from APOGEE. While the spectroscopic orbit was already known for the SB9 stars, this was the case for only one APOGEE star. We tested the difference between a direct calculation of the masses using the orbital parameters and a combined fit using the raw radial velocity measures on SB9. A combined fit estimates the parameters, their uncertainties, and their correlations better. We also estimated the masses of 6 stars resolved by *Gaia* DR3 with literature direct-imaging and either Hipparcos data or literature mass fraction. The dynamical masses of three of these stars were derived for the first time.

The BINARYS tool was used to perform the combined fits. BINARYS was extended for this study to handle *Gaia* DR3 NSS

[3] https://gea.esac.esa.int/archive/documentation/GDR2/Data_processing/chap_cu3ast/sec_cu3ast_cali/ssec_cu3ast_cali_source.html#Ch3.T3

[4] http://perso.ens-lyon.fr/isabelle.baraffe/BHAC15dir/

[5] http://basti-iac.oa-teramo.inaf.it/

Table 3. Solutions for star systems resolved by *Gaia* with direct-imaging data and either HIPPARCOS transit data or literature mass fractions.

Name	$\mathcal{M}_1$	$\sigma_{\mathcal{M}_1}$	$\mathcal{M}_2$	$\sigma_{\mathcal{M}_2}$	ϖ	σ_ϖ	$\rho_{\mathcal{M}_1,\mathcal{M}_2}$	F2
Gl277	0.5276	0.0046	0.2069	0.0031	83.465	0.052	0.77	3.93
Gl330	0.4969	0.0247	0.3184	0.0159	61.513	0.107	0.98	3.37
Gl568	0.3106	0.0067	0.2129	0.0047	87.439	0.069	0.95	1.53
Gl860	0.2915	0.0062	0.1789	0.0046	248.354	1.560	0.39	3.49
Gl65 [(a)]	0.1224	0.0012	0.1195	0.0012	371.396	0.453	−0.28	1.19
Gl473 [(a)]	0.1379	0.0023	0.1258	0.0022	227.041	0.389	−0.76	1.36

Notes. The masses of the primary $\mathcal{M}_1$ and secondary $\mathcal{M}_2$ are given in $\mathcal{M}_\odot$, the parallax ϖ is given in mas, $\rho_{\mathcal{M}_1,\mathcal{M}_2}$ is the correlation between the mass estimates, and F2 is the goodness of fit. [(a)]Solution using the literature mass fraction. The full table including *Gaia* and HIPPARCOS IDs and full orbital solution is available at the CDS.

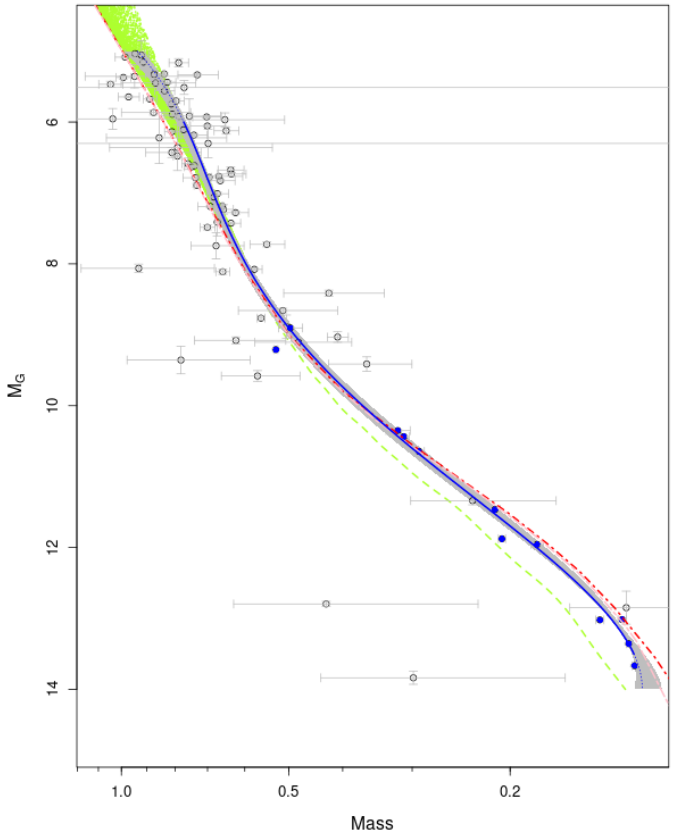

Fig. 8. Mass-luminosity relation fitted in this work (in blue). The areas outside the $6 < M_G < 13.5$ range are shown by the dotted line. The grey area corresponds to the 1σ bootstrap interval. The stars from Table 3 (resolved *Gaia* stars with direct-imaging data) are plotted in blue, and stars from Tables 1 and 2 (SB2 data combined with *Gaia* NSS astrometric solution) are shown in grey. The dashed green lines show the solar metallicity PARSEC isochrones for main-sequence stars (isochrones with the label 1). The dot-dashed red line and the two-dash pink line are the solar metallicity isochrone of Baraffe et al. (2015) and BASTI, respectively; they only deviate at masses lower than $\sim 0.12\,\mathcal{M}_\odot$.

solutions and perspective acceleration within the HIPPARCOS and *Gaia* observation time.

Using the derived masses and the G magnitudes, we derived a first empirical mass-luminosity relation in the G band that took all the correlations between the component masses and magnitudes into account. This empirical relation agrees better with the isochrones of Baraffe et al. (2015) than with the PARSEC isochrones.

Table 4. Coefficient values of the polynomial fit $\log_{10}(\mathcal{M}) = C_0 + C_1 M_G + C_2 M_G^2 + C_3 M_G^3 + C_4 M_G^4$, to be used within $6 < M_G < 13.5$, which corresponds to the $0.12 < \mathcal{M} < 0.77$ mass range.

	Best fit	Upper	Lower
C_0	3.129	3.798	2.534
C_1	−1.5406	−1.8377	−1.2672
C_2	0.27513	0.32373	0.22954
C_3	−0.021661	−0.025067	−0.018413
C_4	0.0005991	0.0006855	0.0005148

Notes. The coefficients are provided for the best fit together with the upper and lower curves at 1σ that were obtained through a bootstrap method.

We expect *Gaia* DR4 to significantly increase the sample of stars that could be used in such a study. Moreover, *Gaia* DR4 will provide access to the epoch astrometry. This will enable a full combined fit on the raw data of spectroscopic or direct-imaging data with *Gaia* astrometry. It will also enable studying systems whose astrometric signal is too low for a full *Gaia* DR4 orbital solution but whose spectroscopic or direct-imaging signal is good. We can therefore expect a much deeper study of the mass-luminosity relation with *Gaia* DR4. In particular, a study of the metallicity dependence should be conducted with a larger sample.

Acknowledgements. We thank J.-B. Le Bouquin for helping debugging our test on HIP 20601 and X. Delfosse for providing lists of close-by M-dwarfs to dig into. We thank S. Cassisi for his prompt feedback on the BASTI isochrones. T.M. is granted by the BELSPO Belgian federal research program FED-tWIN under the research profile Prf-2020-033_BISTRO. This work has made use of data from the European Space Agency (ESA) space mission *Gaia* (https://www.cosmos.esa.int/gaia), processed by the *Gaia* Data Processing and Analysis Consortium (DPAC). Funding for the DPAC is provided by national institutions, in particular the institutions participating in the *Gaia* MultiLateral Agreement. This research has made use of the SIMBAD database, operated at CDS, Strasbourg, France.

References

Arenou, F., Halbwachs, J.-L., Mayor, M., Palasi, J., & Udry, S. 2000, IAU Symp., 200, 135
Babusiaux, C., Fabricius, C., Khanna, S., et al. 2023, A&A, 674, A32
Baraffe, I., Homeier, D., Allard, F., & Chabrier, G. 2015, A&A, 577, A42
Baroch, D., Morales, J. C., Ribas, I., et al. 2018, A&A, 619, A32
Benedict, G. F., Henry, T. J., Franz, O. G., et al. 2016, AJ, 152, 141
Bressan, A., Marigo, P., Girardi, L., et al. 2012, MNRAS, 427, 127
Delfosse, X., Forveille, T., Ségransan, D., et al. 2000, A&A, 364, 217
ESA 1997, The Hipparcos and Tycho Catalogues, SP-1200

Fekel, F. C., Dadonas, V., Sperauskas, J., Vaccaro, T. R., & Patterson, L. R. 1994, AJ, 108, 1936
Fekel, F. C., Williamson, M. H., Muterspaugh, M. W., et al. 2015, AJ, 149, 63
Gaia Collaboration (Arenou, F., et al.) 2023a, A&A, 674, A34
Gaia Collaboration (Vallenari, A., et al.) 2023b, A&A, 674, A1
Geyer, D. W., Harrington, R. S., & Worley, C. E. 1988, AJ, 95, 1841
Ginestet, N., & Carquillat, J. M. 1995, A&AS, 111, 255
Goldberg, D., Mazeh, T., Latham, D. W., et al. 2002, AJ, 124, 1132
Griffin, R. F. 1990, J. Astrophys. Astron., 11, 533
Griffin, R. F. 1993, The Observatory, 113, 294
Griffin, R. F. 2006, MNRAS, 371, 1159
Griffin, R. F. 2008, The Observatory, 128, 95
Griffin, R. F. 2009, The Observatory, 129, 317
Griffin, R. F. 2011, The Observatory, 131, 17
Griffin, R. F. 2012, The Observatory, 132, 356
Griffin, R. F. 2013, The Observatory, 133, 1
Griffin, R. F. 2014, The Observatory, 134, 109
Halbwachs, J. L., Mayor, M., & Udry, S. 2012, MNRAS, 422, 14
Halbwachs, J. L., Mayor, M., & Udry, S. 2018, A&A, 619, A81
Halbwachs, J. L., Kiefer, F., Lebreton, Y., et al. 2020, MNRAS, 496, 1355
Halbwachs, J.-L., Pourbaix, D., Arenou, F., et al. 2023, A&A, 674, A9
Hidalgo, S. L., Pietrinferni, A., Cassisi, S., et al. 2018, ApJ, 856, 125
Imbert, M. 2006, Rom. Astron. J., 16, 3
Jancart, S., Jorissen, A., Babusiaux, C., & Pourbaix, D. 2005, A&A, 442, 365
Kervella, P., Mérand, A., Ledoux, C., Demory, B. O., & Le Bouquin, J. B. 2016, A&A, 593, A127
Kiefer, F., Halbwachs, J. L., Arenou, F., et al. 2016, MNRAS, 458, 3272
Kiefer, F., Halbwachs, J. L., Lebreton, Y., et al. 2018, MNRAS, 474, 731
Kounkel, M., Covey, K. R., Stassun, K. G., et al. 2021, AJ, 162, 184
Kristensen, K., Nielsen, A., Berg, C. W., Skaug, H., & Bell, B. M. 2016, J. Stat. Softw., 70, 1
Lallement, R., Vergely, J. L., Babusiaux, C., & Cox, N. L. J. 2022, A&A, 661, A147
Leclerc, A., Babusiaux, C., Arenou, F., et al. 2023, A&A, 672, A82
Lindegren, L., Bastian, U., Biermann, M., et al. 2021, A&A, 649, A4
Majewski, S. R., Schiavon, R. P., Frinchaboy, P. M., et al. 2017, AJ, 154, 94
Mann, A. W., Dupuy, T., Kraus, A. L., et al. 2019, ApJ, 871, 63
Mason, B. D., Hartkopf, W. I., Miles, K. N., et al. 2018, AJ, 155, 215
Mayor, M., & Turon, C. 1982, A&A, 110, 241
Mazeh, T., Martin, E. L., Goldberg, D., & Smith, H. A. 1997, MNRAS, 284, 341
McAlister, H. A., Hartkopf, W. I., Sowell, J. R., Dombrowski, E. G., & Franz, O. G. 1989, AJ, 97, 510
Mermilliod, J. C., Mayor, M., & Udry, S. 2009, A&A, 498, 949
Piccotti, L., Docobo, J. Á., Carini, R., et al. 2020, MNRAS, 492, 2709
Pourbaix, D. 2000, A&AS, 145, 215
Pourbaix, D., Tokovinin, A. A., Batten, A. H., et al. 2004, A&A, 424, 727
Sperauskas, J., Deveikis, V., & Tokovinin, A. 2019, A&A, 626, A31
Tokovinin, A. 2019, AJ, 158, 222
Tomkin, J. 2005, The Observatory, 125, 232
Tomkin, J. 2007, The Observatory, 127, 165
Torres, G., Henry, T. J., Franz, O. G., & Wasserman, L. H. 1999, AJ, 117, 562
van Leeuwen, F. 2007, Hipparcos, the New Reduction of the Raw Data, 350
Wilson, E. B., & Hilferty, M. M. 1931, Proc. Natl. Acad. Sci., 17, 684

Appendix A: Direct calculation process for SB9

Because the orbital parameters are both given by SB9 and Gaia, it is easy to combine astrometry with spectroscopy. The features of the star systems were directly computed from the astrometric and spectroscopic orbital solutions, using commonly used formulae. This direct-calculation method is approximately the same as the method that was applied to calculate the mass by the Gaia collaboration (Gaia Collaboration 2023a).

From the semi-amplitudes given by spectroscopy, the mass ratio is

$$q = \frac{\mathcal{M}_2}{\mathcal{M}_1} = \frac{K_1}{K_2}. \tag{A.1}$$

The dynamical mass of the secondary is

$$\mathcal{M}_2 = 1.0385 \times 10^{-7} K_1^3 P (1-e^2)^{3/2} \left(1+\frac{1}{q}\right)^2 \frac{1}{\sin^3 i}, \tag{A.2}$$

where P is the period in days, K_1 is given in km.s^{-1}, and the inclination i is given by the Gaia astrometry. The period and the eccentricity e were the weighted mean of the Gaia and SB9 values.

The primary mass was then deduced from the mass ratio and the secondary mass.

The flux fraction of the secondary $\beta = \frac{F_2}{F_1+F_2}$ is given through the relation between the individual stars orbits and the photocentre orbit provided by astrometry,

$$a_0 = (B-\beta)\, a_{21}, \tag{A.3}$$

where B is the mass fraction of the secondary,

$$B = \frac{\mathcal{M}_2}{\mathcal{M}_1+\mathcal{M}_2} = \frac{q}{1+q}, \tag{A.4}$$

a_{21} is the semi-major axis of the relative orbit between the primary and the secondary,

$$a_{21} = a_1 + a_2 = a_1\left(1+\frac{1}{q}\right), \tag{A.5}$$

and a_0 is the semi-major axis of the photocentre orbit.

Here, $a_{1/2}$ are the individual semi-major axis of the primary and secondary, respectively. They can be deduced from the semi-amplitudes,

$$a_{1,2} = \frac{1}{10879} K_{1,2} P \frac{\sqrt{1-e^2}}{\sin i}, \tag{A.6}$$

where the semi-major axis is given in au and the period in days.

The masses $\mathcal{M}_1$, $\mathcal{M}_2$, and the flux fraction β are then obtained through Eq. 2, 3, 4 respectively.

Astrometry is needed here to determine the photocentre orbit a_0, but also to convert it from mas into au using the parallax ϖ.

The errors were estimated through a Monte Carlo method (with $n_{MC} = 10^3$) assuming all the parameter distributions to be Gaussian-like. The Gaia parameters were generated simultaneously according to the covariance matrix, except for the photocentre semi-major axis a_0. Its error has been shown by Babusiaux et al. (2023) to be over-estimated by a Monte Carlo approach, and the local linear approximations of Halbwachs et al. (2023) was used for it. In order to take potential asymmetry in the final parameter distributions into account, the lower and upper confidence levels were determined at 16% and 84%. The results of this direct calculation are listed in Table A.1.

Appendix B: Jacobian calculations

The TMB algorithm provides as output the orbital parameters with their associated uncertainties, in particular, the period P with σ_P and the parallax ϖ with σ_ϖ. It additionally gives the semi-major axis of the primary orbit a_1 with its error σ_{a1}, the mass ratio q with σ_q , and the flux fraction β with σ_β. The global covariance matrix is also calculated.

Using $a_2 = \frac{a_1}{q}$, we derived the masses with

$$\mathcal{M}_1 = \frac{(a_1+a_2)^3}{P^2\,(1+q)} = \frac{a_1^3\,(1+q)^2}{P^2\,q^3} \tag{B.1}$$

$$\mathcal{M}_2 = \frac{(a_1+a_2)^3 q}{P^2\,(1+q)} = \frac{a_1^3\,(1+q)^2}{P^2\,q^2}, \tag{B.2}$$

and the magnitudes were obtained through Eq. 8 and Eq. 9 from the parameters (ϖ, β) as well as the apparent magnitude G and the absorption A_G. The last two are independent and independent of the other parameters. For simplicity, we therefore considered here only the extinction-corrected magnitude $G_0 = G - A_G$, which has a variance of $\sigma^2_{G_0} = \sigma^2_G + \sigma^2_{A_G}$.

The covariance of the parameters $(a_1, q, P, \varpi, \beta)$ Σ_{TMB} are provided by TMB. The full covariance of our input parameters $(a_1, q, P, \varpi, \beta, G_0)$ is then

$$\Sigma_{params} = \begin{pmatrix} \Sigma_{TMB} & 0 \\ 0 & \sigma^2_{G_0} \end{pmatrix}. \tag{B.3}$$

The covariance of our output parameters $(\mathcal{M}_1, \mathcal{M}_2, M_{G_1}, M_{G_2})$, Σ, is then

$$\Sigma = J^T\, \Sigma_{params}\, J$$

with J the Jacobian of the transformation from $(a_1, q, P, \varpi, \beta, G_0)$ to $(\mathcal{M}_1, \mathcal{M}_2, M_{G_1}, M_{G_2})$,

$$J = \begin{pmatrix} \partial_{a_1}\mathcal{M}_1 & \partial_{a_1}\mathcal{M}_2 & 0 & 0 \\ \partial_q\mathcal{M}_1 & \partial_q\mathcal{M}_2 & 0 & 0 \\ \partial_P\mathcal{M}_1 & \partial_P\mathcal{M}_2 & 0 & 0 \\ 0 & 0 & \partial_\varpi M_{G_1} & \partial_\varpi M_{G_2} \\ 0 & 0 & \partial_\beta M_{G_1} & \partial_\beta M_{G_2} \\ 0 & 0 & \partial_{G_0} M_{G_1} & \partial_{G_0} M_{G_2} \end{pmatrix}. \tag{B.4}$$

The derivatives of the primary mass are given in the equations below,

$$\partial_{a_1}\mathcal{M}_1 = \frac{3a_1^2\,(1+q)^2}{P^2\,q^3} \tag{B.5}$$

$$\partial_q\mathcal{M}_1 = \frac{a_1^3}{P^2}\left(\frac{2(1+q)}{q^3} - \frac{3(1+q)^2}{q^4}\right) \tag{B.6}$$

$$\partial_P\mathcal{M}_1 = -2\frac{a_1^3\,(1+q)^2}{P^3\,q^3}. \tag{B.7}$$

The derivatives of the secondary mass are given in the equations below,

$$\partial_{a_1}\mathcal{M}_2 = \frac{3a_1^2\,(1+q)^2}{P^2\,q^2} \tag{B.8}$$

Table A.1. Results from direct calculation for SB9

Gaia DR3 ID	$\mathcal{M}_1$	$\sigma_{\mathcal{M}_1}$	$\mathcal{M}_{1_{low}}$	$\mathcal{M}_{1_{up}}$	$\mathcal{M}_2$	$\sigma_{\mathcal{M}_2}$	$\mathcal{M}_{2_{low}}$	$\mathcal{M}_{2_{up}}$	β	σ_β	β_{low}	β_{up}
48197783694869760	0.994	0.038	0.954	1.031	0.679	0.022	0.656	0.700	0.101	0.001	0.097	0.105
69883417170175488	0.895	0.024	0.873	0.920	0.843	0.021	0.822	0.863	0.399	0.003	0.394	0.404
308256610357824640	0.440	0.341	0.168	0.478	0.312	0.241	0.119	0.338	0.283	0.010	0.233	0.288
478996438146017280	0.778	0.022	0.753	0.797	0.717	0.020	0.694	0.734	0.385	0.002	0.382	0.388
544027809281308544	0.954	0.059	0.897	1.018	0.796	0.036	0.761	0.833	0.137	0.001	0.131	0.144
595390807776621824	0.788	0.011	0.777	0.799	0.695	0.007	0.687	0.702	0.309	0.001	0.307	0.312
660622010858088320	0.715	0.065	0.656	0.783	0.626	0.038	0.588	0.665	0.227	0.003	0.217	0.237
827608625636174720	0.776	0.051	0.726	0.823	0.730	0.049	0.682	0.775	0.408	0.003	0.404	0.412
882872210352301568	1.007	0.011	0.996	1.018	0.506	0.003	0.503	0.509	0.025	0.001	0.021	0.029
1067685718250692352	1.035	0.013	1.022	1.048	0.919	0.012	0.908	0.931	0.300	0.002	0.294	0.305
1074883087005896320	0.641	0.037	0.608	0.680	0.602	0.034	0.572	0.638	0.396	0.005	0.389	0.403
1324699172583973248	1.309	0.056	1.254	1.365	1.154	0.044	1.109	1.198	0.315	0.002	0.311	0.319
1441993625629660800	1.116	0.046	1.062	1.151	0.932	0.028	0.897	0.951	0.092	0.001	0.084	0.098
1480959875337657088	0.864	0.257	0.655	1.122	0.811	0.169	0.664	0.978	0.291	0.014	0.258	0.324
1517219363639758976	1.114	0.053	1.066	1.170	0.913	0.042	0.875	0.958	0.163	0.001	0.157	0.170
1517927895803742080	0.584	0.013	0.571	0.597	0.549	0.017	0.533	0.566	0.361	0.002	0.357	0.365
1528045017687961856	1.125	0.030	1.095	1.154	0.764	0.019	0.744	0.783	0.068	0.001	0.064	0.071
1615450866336763904	1.000	0.045	0.956	1.044	0.787	0.031	0.757	0.816	0.131	0.001	0.125	0.136
1918953867019478144	1.040	0.006	1.036	1.047	0.969	0.005	0.964	0.974	0.390	0.001	0.388	0.392
2012218158438964224	2.072	0.129	1.957	2.207	1.952	0.119	1.848	2.078	0.338	0.004	0.331	0.345
2035577729682322176	0.708	0.048	0.664	0.759	0.641	0.044	0.602	0.687	0.326	0.003	0.321	0.332
2067948245320365184	0.839	0.002	0.837	0.842	0.660	0.002	0.658	0.662	0.153	0.001	0.151	0.154
2129771310248902016	0.748	0.038	0.712	0.785	0.672	0.032	0.640	0.702	0.316	0.002	0.311	0.321
2185171578009765632	1.190	0.030	1.160	1.218	1.093	0.032	1.059	1.124	0.412	0.005	0.405	0.419
2198442167969655296	1.021	0.046	0.976	1.067	0.772	0.027	0.745	0.800	0.203	0.001	0.198	0.208
3283823387685219328	1.017	0.019	0.995	1.032	0.755	0.014	0.739	0.766	0.124	0.004	0.093	0.151
3312631623125272448	0.990	0.077	0.925	1.076	0.700	0.054	0.655	0.761	0.139	0.002	0.128	0.150
3366718833479009408	1.050	0.011	1.038	1.061	0.673	0.006	0.667	0.679	0.017	0.001	0.012	0.022
3409686270424363008	0.794	0.016	0.778	0.811	0.561	0.010	0.551	0.571	0.105	0.001	0.102	0.109
3427930123268526720	0.933	0.087	0.849	1.018	0.308	0.029	0.282	0.336	0.074	0.001	0.067	0.079
3536759371865789568	1.588	0.075	1.514	1.662	1.380	0.051	1.331	1.428	0.208	0.002	0.201	0.214
3549833939509628672	0.957	0.042	0.916	1.001	0.900	0.032	0.868	0.931	0.359	0.004	0.352	0.366
3931519127529822208	1.085	0.076	1.015	1.164	0.838	0.034	0.806	0.872	0.144	0.001	0.139	0.148
3935131126305835648	1.418	0.086	1.338	1.507	0.998	0.060	0.942	1.061	0.135	0.001	0.129	0.141
3954536956780305792	0.694	3.100	0.262	0.933	0.629	2.756	0.238	0.853	0.333	0.019	0.271	0.352
3964895043508685312	0.674	0.183	0.531	0.835	0.599	0.163	0.473	0.743	0.218	0.006	0.198	0.236
4145362250759997952	1.492	0.400	1.145	1.929	0.956	0.191	0.782	1.154	0.105	0.003	0.079	0.133
4228891667990334976	1.294	0.095	1.192	1.376	1.116	0.081	1.029	1.187	0.304	0.002	0.300	0.308
4354357901908595456	0.756	0.067	0.693	0.825	0.428	0.023	0.408	0.452	0.060	0.001	0.056	0.064
4589258562501677312	0.681	0.066	0.617	0.750	0.559	0.041	0.520	0.600	0.292	0.003	0.284	0.300
5762455439477309440	0.802	0.069	0.739	0.874	0.646	0.034	0.613	0.680	0.177	0.002	0.169	0.185
6244076338858859776	0.776	0.015	0.760	0.790	0.684	0.011	0.673	0.694	0.294	0.001	0.291	0.296
6799537965261994752	0.892	0.006	0.890	0.900	0.802	0.005	0.801	0.809	0.326	0.002	0.322	0.331

$$\partial_q \mathcal{M}_2 = \frac{a_1^3}{P^2}\left(\frac{2(1+q)}{q^2} - \frac{2(1+q)^2}{q^3}\right) \tag{B.9}$$

$$\partial_P \mathcal{M}_2 = -2\frac{a_1^3\,(1+q)^2}{P^3\,q^2}. \tag{B.10}$$

As a reminder, the absolute magnitudes are given by the Eq. 8 and 9.

The derivatives of the primary magnitude are given below,

$$\partial_\varpi M_{G_1} = \frac{5}{\log(10)}\frac{1}{\varpi} \tag{B.11}$$

$$\partial_\beta M_{G_1} = \frac{2.5}{\log(10)}\frac{1}{1-\beta} \tag{B.12}$$

$$\partial_{G_0} M_{G_1} = 1. \tag{B.13}$$

The derivatives of the secondary magnitude are given below,

$$\partial_\varpi M_{G_2} = \frac{5}{\log(10)}\frac{1}{\varpi} \tag{B.14}$$

$$\partial_\beta M_{G_2} = -\frac{2.5}{\log(10)}\frac{1}{\beta} \tag{B.15}$$

$$\partial_{G_0} M_{G_2} = 1. \tag{B.16}$$